Grant number: 101057622

SEAWave

Project**: SEAWave**

Translation of downlink incident field

Work Package: WP1

Deliverable: D1.3

Deliverable No.: D3

Abstract

In this deliverable we present the methodology for implementing an integrative approach to evaluate global exposure. We present the numerical techniques that allow the conversion of incident field to power and cumulative energy absorption in the tissues. The corresponding metrics are expressed in W/kg andJ/kg. The methodology is implemented as an example in the case of native voice calls.

Project Details

Project name	SEAWave
Grant number	101057622
Start Date	01 Jun 2022
Duration	42 months
Scientific coordinator	Prof T Samaras, Aristotle University of Thessaloniki (AUTH)

Deliverable Details

Deliverable related number	D1.3
Deliverable No.	D3
Deliverable name	Translation of downlink incident fields
Work Package number	WP1
Work Package name	Exposures from 5G vs. 2G–4G Cellular Networks
Authors	Shanshan Wang, Joe Wiart (TP-IPP) Theodoros Samaras (AUTH)
Distribution	Public
Version	1
Draft/final	Final
Keywords	EMF global exposure, downlink, absorbed power, organ-averaged SAR, cumulative exposure, organ-averaged SA

Table of Contents

1. Numerical methods used to assess exposure

1.1. Maxwell's equations and numerical methods for dosimetry

Maxwell's equations [1, 2] govern the relationship between the electric and magnetic components of the electromagnetic field. These equations may have analytical solutions for plane waves or spherical waves, but most of the time they do not have an analytical solution in complex media. For this reason, the solution is often obtained using numerical simulations, i.e., computational electromagnetics.

Recent advances in high-performance computing (HPC) using parallel architecture or graphics processing units (GPUs) have allowed numerical techniques to be used intensively (Figure 1.1), and in particular to assess exposure to radiofrequency (RF) electromagnetic fields (EMF).

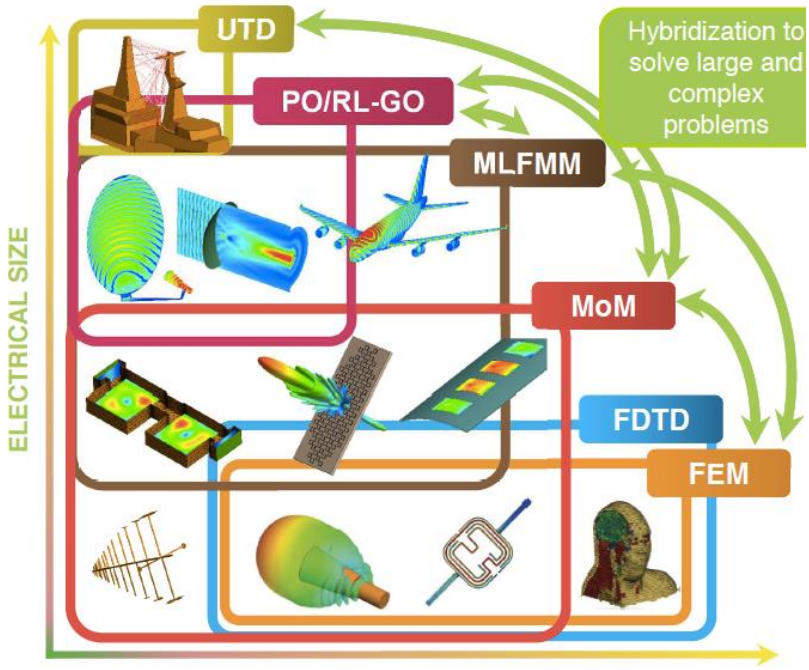

Figure 1.1. Numerical techniques in computational electromagnetics

Commercial codes based on various methods, such as the finite element method (FEM) or finite differences in the time domain method (FDTD [3], TLM [4], and FIT [5]), are now available. FDTD uses the discretization of Maxwell's equations in their differential form. FIT, on the other hand, is based on the discretization of Maxwell's equations in their integral form.

In the field of radiofrequencies, the high heterogeneity of tissues has led researchers to use approaches that do not require matrix inversion. Finite difference-based methods (FDTD, TLM, and FIT) have therefore been used extensively to design systems and assess human exposure

induced by equipment radiating electromagnetic waves. To perform these simulations in the field of bioelectromagnetics, the most widely used solution method is the finite difference time-domain method (FDTD). This method can handle very large problems with high heterogeneity, as is the case with a human being. Its formalism is also well-suited to voxelized models from medical imaging.

There is a wealth of literature on the FDTD method. We will briefly review the basics of FDTD performed on a discretized space with an orthogonal mesh. The electric and magnetic field vectors are sampled on a temporal and spatial grid [6]. With this method the vectors $\vec{E}$ and $\vec{H}$ are represented by six matrices $\{E_x, E_y, E_z, H_x, H_y, H_z\}$ of their components sampled at different points x_i, y_j, z_k and times t_n. The vector components may or may not be colocated [7].

Discretization schemes can be implicit or explicit. Implicit approaches require matrix inversion, which is not suitable for very large problems. Explicit schemes are used to solve Maxwell's equations through an iterative process that does not require matrix inversion. Their stability depends on adherence to certain constraints.

Numerous studies have been conducted [8], providing stability conditions through a relationship between the time increment, dt, and the spatial mesh dx, dy, dz. In the case of a uniform mesh, this in a medium with phase velocity ν the stability condition is:

$$dt \leq \frac{1}{\nu\sqrt{\frac{1}{dx^2}+\frac{1}{dy^2}+\frac{1}{dz^2}}}$$

The sampling model influences the accuracy of the approximation. Centered finite differences have a significant advantage since, as the following equations show, they provide second-order accuracy for the derivative estimation.

$$\frac{\partial f}{\partial x}(x_0) = \frac{f(x_0 + h/2) - f(x_0 - h/2)}{h} + \mathcal{O}(h^2)$$

A higher-order scheme can be used [9] but the computational effort is much greater. The most popular FDTD scheme is the Yee scheme with spatial sampling, illustrated in Figure 1.2, and known as the ‘Yee cell’. The Yee approach is based on sampling the non-co-localized components of electric and magnetic field in space and time, which involves an interlacing known as ‘leapfrog’.

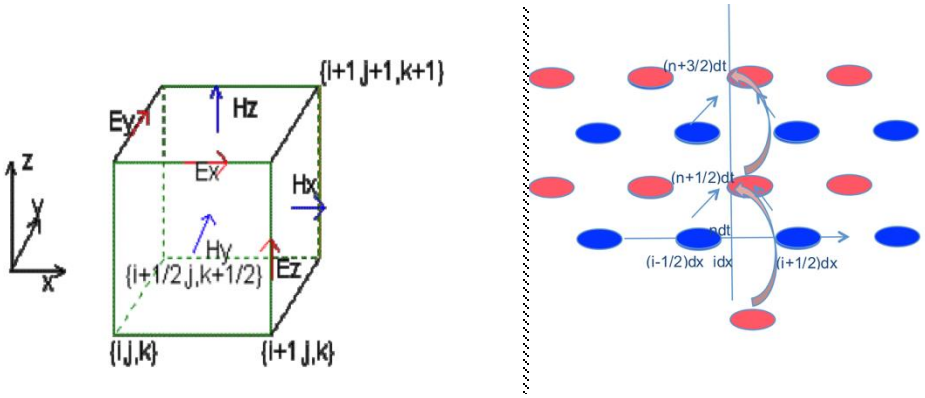

Figure 1.2. Yee cell and leapfrog scheme

Evaluating the specific absorption rate (SAR) in a given voxel (identical to a Yee cell) requires knowing not only the dielectric properties of the cell's constituent medium, but also the electric field strength within the cell. The FDTD provides the electric field components E at the edges of the Yee cell; therefore, these components must be interpolated to evaluate the electric field strength E involved in calculating the SAR in each cell (Figure 1.3). An IEC/IEEE standard [10]is dedicated to controlling the uncertainty of the SAR assessment by the FDTD.

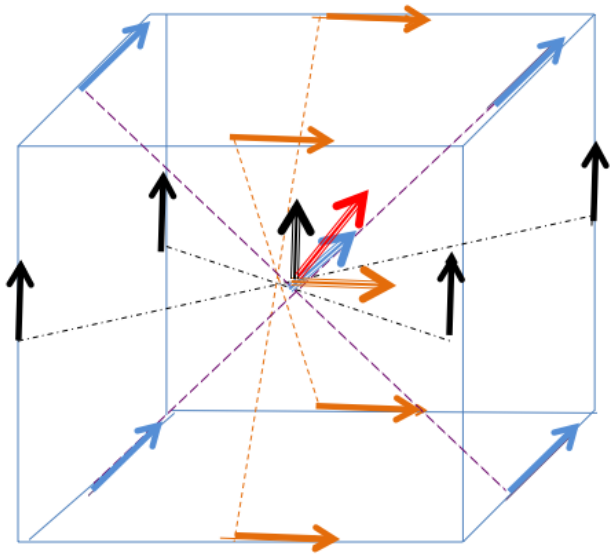

Figure 1.3. Electric field strength estimation in the centre of the Yee cell

1.2. Computational human models

Digital, or computer-generated, models of human beings can be classified into four main categories. The first, and oldest, category includes ‘mathematical’ models [11, 12, 13, 14, 15,16] composed of spheres, cylinders, cones, ellipsoids, and elliptical cylinders. These ‘stylized’ models

were primarily used for studies of exposure to ionizing radiation. They were relatively easy to implement but of limited use for RF exposure because the anatomical shapes of the body and organs are important in this field. In the RF domain, the first anatomical and mathematical model was "Blockman" [17]composed of 180 cells of different sizes arranged to best fit the contour of a man but the resolution of "Blockman" and the description of the internal organs is not really compatible with the frequency used in wireless communication systems.

The second category consists of models based on computed tomography (CT) scans taken during a medical examination [18,19]. This method uses ionizing radiation, and the images are very often limited to organs. The third category includes models based on CT scans and photographic images of deceased individuals who donated their bodies [20, 21, 22, 23, 24, 25]. The best known is certainly "Visible Man," whose images have been used in many biomedical applications. These models have very good resolution and are anatomically correct, but for ethical reasons, few models exist.

The last category consists of models based on magnetic resonance imaging (MRI). In the RF domain, most of the anatomically correct and heterogeneous digital models of adults used today are based on magnetic resonance imaging (MRI) data.

The aim of this section is not to provide an exhaustive description of all existing models but to provide information on the most commonly used models.

In the United States, two human voxel models were developed. The first, called "Zubal" [26], had a resolution of 4mm × 4mm × 4mm, and the second, known as "Visible Human" [27], had millimetre resolution. In the United Kingdom, two models, a male known as "Norman" and a female known as "Naomi," based on MRI images, were developed [28, 29] with a spatial resolution of 2mm × 2mm × 2mm. In Japan, models of adult Japanese men and women [30], known as "Taro" and "Hanako," were also developed based on MRI. The models are composed of 50 different tissues and organs with a spatial resolution of 2mm × 2mm × 2mm. In Korea, two adult male models were constructed based on MRI [31]and another on photographic images [32]. In China, two adult models (male and female) were developed [33]with a resolution of 1mm × 1mm × 1mm, with 90 and 87 identified tissues/organs for the female and male model, respectively. Figure 1.4 illustrates some of the available anatomical models.

In Europe, models [34], based on MRI images, have been developed since 2010. They are part of the “virtual family”; these models [35], were composed of more than 80 tissues in 2010, and today they comprise more than 300 tissues. These models have millimetre and sometimes submillimetre resolution.

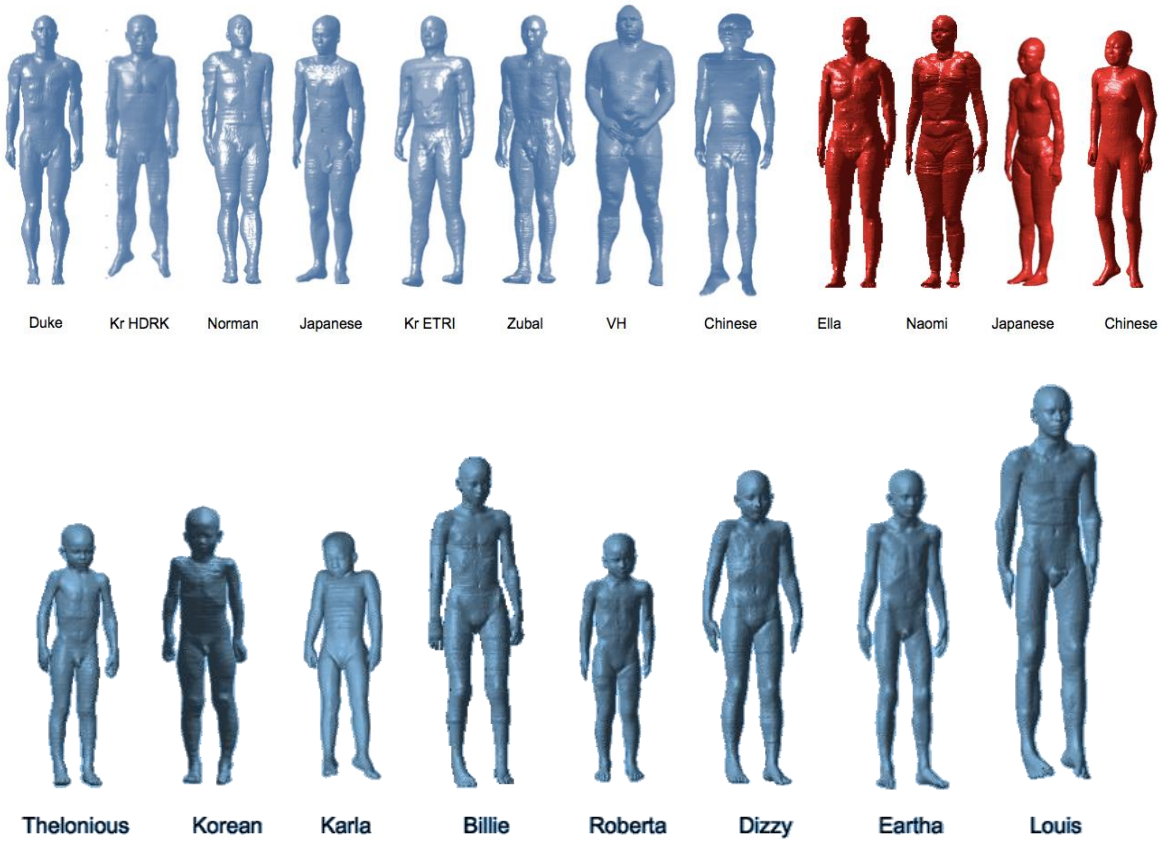

Figure 1.4. Examples of computational human phantoms (adults and children)

2. Exposure induced by Downlink emission.

2.1. From downlink incident field to organ exposure

The SAR induced by an incident plane wave cannot be assessed experimentally. As pointed out in section 1 the SAR induced by an incident plane wave can be evaluated via numerical simulations. We computed SAR distributions using Sim4Life (ZMT, Zurich, Switzerland), an FDTD solver for Maxwell's equations. This approach remains the gold standard for bioelectromagnetic simulations due to its ability to handle complex anatomical geometries, heterogeneous tissue dielectric properties, and dynamic near-field interactions.

2.2. Numerical human models used in SEAWave

As explained previously the selection of an appropriate computational human model is critical for accurate simulations, as both anatomical representativeness and spatial resolution directly influence the reliability of absorbed power calculations. In SEAWave we used four models from the Virtual Family: Duke, Ella, Louis, and Eartha. These models, derived from high-resolution Magnetic Resonance Imaging (MRI) scans (1mm × 1mm × 1mm isotropic voxels). Duke for instance represents a 34- year-old male with standard anthropometry (1.77 m, 70 kg).

2.3. Simulation results

Duke

Tissue or organ (used for averaging)	Frequency (MHz)					Comments
	900	1800	2600	3500	5500	all values of the table in (mW/kg)/(W/m^2)
Whole body	4,79	4,06	3,46	2,85	2,09	
Head	7,38	5,46	4,40	3,80	3,01	above chin
Skin	12,32	15,21	16,56	16,60	16,89	
Brain	9,16	3,90	2,05	1,12	0,20	white and grey matter, CSF, cerebellum, etc.
Grey matter	8,67	4,07	2,26	1,26	0,21	
White matter	6,07	2,53	1,12	0,49	0,05	
Gonads	11,67	11,09	11,25	8,64	3,01	testicles in male and ovaries in female models

Ella

Tissue or organ (used for averaging)	Frequency (MHz)					Comments
	900	1800	2600	3500	5500	all values of the table in (mW/kg)/(W/m^2)
Whole body	5,89	4,32	3,14	2,52	1,87	
Head	7,36	6,22	4,46	3,65	2,38	above chin
Skin	18,85	15,44	11,15	8,10	6,11	
Brain	8,74	6,33	4,04	3,35	1,85	white and grey matter, CSF, cerebellum, etc.
Grey matter	7,85	5,67	3,54	3,00	1,72	
White matter	5,34	3,80	2,33	1,94	1,07	
Gonads	0,86	0,31	0,26	0,28	0,19	testicles in male and ovaries in female models

Louis

Tissue or organ (used for averaging)	Frequency (MHz)					Comments
	900	1800	2600	3500	5500	all values of the table in (mW/kg)/(W/m^2)
Whole body	5,92	4,91	3,89	2,96	1,99	
Head	7,10	6,07	4,56	3,67	2,35	above chin
Skin	14,04	13,87	11,65	8,66	5,93	
Brain	8,39	6,26	3,92	3,23	1,96	white and grey matter, CSF, cerebellum, etc.
Grey matter	8,08	6,13	3,85	3,28	2,06	
White matter	6,10	4,65	2,71	2,21	1,41	
Gonads	11,39	11,67	14,75	12,78	5,23	testicles in male and ovaries in female models

Eartha

Tissue or organ (used for averaging)	Frequency (MHz)					Comments
	900	1800	2600	3500	5500	all values of the table in (mW/kg)/(W/m^2)
Whole body	7,48	5,81	4,46	3,40	2,57	
Head	7,68	5,86	4,26	3,57	2,84	above chin
Skin	16,17	14,61	11,69	8,64	6,50	
Brain	8,67	5,96	3,69	3,21	2,47	white and grey matter, CSF, cerebellum, etc.
Grey matter	8,89	6,14	3,82	3,38	2,80	
White matter	6,38	4,41	2,66	2,27	1,96	
Gonads	2,41	1,61	1,04	0,70	0,32	testicles in male and ovaries in female models

2.4. Comparison of cumulative exposure from mobile devices and network infrastructure

Using the results presented in deliverable D1.1 (D1 “Analysis of downlink incident field and nearby users”) and deliverable D1.2 (D2 “Characterisation of use patterns and user posture of wireless ICT devices”) we can attempt a comparison between the exposure to RF-EMF resulting from the user wireless devices (mobile phones/smartphones) and cellular network infrastructure (base stations) in an urban environment.

The results of numerical simulations show that the specific absorption rate (SAR) averaged over the head of each numerical human model when the phone is next to their ear (voice call) varies with frequency (Table 2.1). To obtain these results we assume that (according to the SEAWave measurement campaigns) the phones operating in 4G and 5G networks use on average a transmission power of 8 mW (i.e., 3.2% of the maximum of 250 mW, see Table 3.3 of Deliverable 1.2). We do not consider at all 2G voice calling, for which the average transmission power is several times higher (in the order of 80 mW).

Table 2.1. Head-averaged SAR for phone next to the ear when making a native voice call (4G/5G)

Human Phantom	Sex	Age [years]		Frequency [MHz]			
				900	1800	2600	3500
Duke	male	34	SAR [µW/kg]	1375.1	142.7	82.2	109.3
Ella	female	26		551.6	162.9	98.3	124.1
Louis	male	14		242.5	153.2	118.8	140.0
Eartha	female	8		620.2	166.3	110.7	145.6

Taking into consideration that the median native voice calls (total of incoming and outgoing) in Europe amount to 350 minutes per month (Deliverable 1.2) the head-averaged specific absorption per day ("cumulative exposure" or "dose") is given in Table 2.2, considering that the above use time is equally distributed among 30 days, resulting in a use of 700 seconds per day.

Table 2.2. Head-averaged specific absorption per day for phone next to the ear when making a native voice call (4G/5G)

Human Phantom	Sex	Age [years]		Frequency [MHz]			
				900	1800	2600	3500
Duke	male	34	SA [mJ/kg]	963	100	58	76
Ella	female	26		386	114	69	87
Louis	male	14		170	107	83	95
Eartha	female	8		434	116	77	102

In order to calculate the exposure to RF-EMF from cellular network infrastructure (base stations) we need to assess the median value for outdoor and indoor exposure. In the case of countries that have adopted the ICNIRP guidelines (and not stricter limits, like in Belgium or Switzerland), SEAWave measurement campaigns indicate that the total incident electric field (rms) is 1 V/m outdoors, which corresponds to a plane wave equivalent incident power density of 2.65 mW/m^2. This total power density is distributed differently in the frequency bands in different countries, depending on spectrum licensing, strategy of network deployment, as well as network architecture of each operator. Therefore, it is difficult to evaluate a median exposure index in each frequency band, so we assume that this total power density is equally distributed among the frequency bands for which we have numerical results.

Another difficult issue is the evaluation of the total equivalent power density indoors from base stations. The measurements performed during SEAWave have shown that the average incident electric field (rms) in public places and transportation can reach 0.5 V/m, which corresponds to a plane wave equivalent incident power density of 0.66 mW/m^2. We can assume that 70% of the day we spent indoors in places with this incident power density (again equally distributed among the frequency bands). With these assumptions we calculate the specific absorption rate averaged over the head (Table 2.3). The cumulative exposure (specific absorption) per day (86'400 seconds) is given in Table 2.4.

Table 2.3. Head-averaged SAR for exposure to downlink signals (weighted average of indoor/outdoor exposure)

Human Phantom	Sex	Age [years]		Frequency [MHz]			
				900	1800	2600	3500
Duke	male	34	SAR [µW/kg]	9.3	6.9	5.5	4.8
Ella	female	26		9.3	7.8	5.6	4.6
Louis	male	14		8.9	7.6	5.7	4.6
Eartha	female	8		9.7	7.4	5.4	4.5

Table 2.4. Head-averaged specific absorption per day for exposure to downlink signals (weighted average of indoor/outdoor exposure)

Human Phantom	Sex	Age [years]		Frequency [MHz]			
				900	1800	2600	3500
Duke	male	34	SA [mJ/kg]	802	593	478	413
Ella	female	26		800	675	484	396
Louis	male	14		771	659	495	399
Eartha	female	8		834	637	462	388

Since it is not possible to evaluate with accuracy the amount of time the phone operates in each frequency band, we can assume a daily cumulative exposure from the phone that is the average of the values over all frequencies in Table 2.2. Moreover, the distribution of the incident power density in the different frequency bands depends on the environment, the architecture of the cellular network, the strategy of deployment of the operator etc.; therefore, the values of Table 2.4 can also be averaged over all frequencies to obtain the cumulative exposure to downlink fields in a day. The comparison of head cumulative exposure to uplink (mobile device) and downlink (network infrastructure) signals is given in Table 2.5.

Table 2.5. Comparison of head-averaged cumulative exposure in a day

Human Phantom	Sex	Age [years]		UL	DL
Duke	male	34	SA [mJ/kg] per day	299	571
Ella	female	26		164	589
Louis	male	14		114	581
Eartha	female	8		182	580

At this point we attempt a validation of our calculations. Lee and Choi published in 2023 an article with a similar but more intricate methodology to evaluate the cumulative exposure per day of the whole brain of children and adults [36]. Their methodology was more refined because they weighted their results with the measured values of UL transmission power and DL environmental fields in each frequency range.

They used a 10 minutes per day phone time, which is not substantially different from the 11.67 minutes per day that we assumed. However, the phone transmitted power they assumed for uplink was 0.1-0.25 mW which is far smaller than the 8 mW of our measurements in SEAWave. Moreover, they did not report on a total plane wave equivalent power density but gave a value for it in each frequency range. The total power density of DL environmental fields amounted to 0.46 mW/m^2, much lower than the 2.65 mW/m^2 that we assumed in our calculations. However, the authors did not distinguish between indoor and outdoor exposure.

If we apply all the above parameters of Lee and Choi [36] to our cumulative exposure calculations, we end up with a specific absorption per day of 0.5 mJ/kg and 214 mJ/kg, for UL and DL, respectively, for the model of Eartha who is an 8-year-old child. This compares reasonably with the respective values of 2 mJ/kg and 300 mJ/kg for the KR-6-WB model of a 6-year-old child reported by Lee and Choi [36]. For the comparison of adult models, we use Ella whose anthropometry is closer to the adult model of KR-22-WB. The specific absorption per day of Ella is 0.5 mJ/kg and 223 mJ/kg, for UL and DL, respectively, which compares better with 1 mJ/kg and 230 mJ/kg of KR-22 in [36].

Therefore, our transfer functions for translating exposure to cumulative exposure in a day can be considered valid, given the approximations of averaging and the assumptions we have applied.

Combining the above methodology for the whole-body results with the methodology in [37], the global exposure index (EI) for a hypothetical mobile use scenario (with known use characteristics) and for each of the four human models can be calculated.

3. Conclusions

Two conclusions emerge from the results reported in this deliverable and those in deliverables D1.1 (D1) and D1.2 (D2):

- Exposure to direct radiation (DL) from base station antennas is well below the limits (a few thousand times). Referring to the table for Louis in section 2.3, the maximum whole-body exposure induced by an incident DL field (related to the base station) in the frequency band from 700 MHz to 3500 MHz is 0.0060 mW/kg for an adult and 0.0094 mW/kg for a child, which is significantly lower than the ICNIRP recommendations (0.08 W/kg, or 80 mW/kg), even when taking an integrative approach and calculating the global exposure index. If we do not assume indoor/outdoor weighting but use the median value for outdoor DL fields in Europe the above values become 0.0127 mW/kg for an adult and 0.0198 mW/kg for a child, values which are still substantially lower than the basic limits in exposure guidelines.
- Comparing the average specific absorption rate (SAR) over the head in Tables 2.1 and 2.3 it is clear the exposure to the radiation of the mobile device (UL) is at least one order of magnitude higher than the exposure to the environmental fields of cellular networks (DL). However, if one calculates the average specific absorption (SA) in the head over one day, also known as cumulative exposure or dose, the two radiation sources contribute to the result with the same order of magnitude (Table 2.5). However, the ratio of the contribution can change if other assumptions are applied for the parameters of exposure (see [36]).
- This study, therefore, concludes that exposure to RF-EMF induced by mobile phones and base stations is very low compared to exposure guidelines but tends to equalize for 4G/5G systems. It should be noted that for the cumulative exposure from the mobile device only native voice calls were accounted for. Including other applications/services will increase this cumulative exposure in the day, bringing it closer to the cumulative exposure from a base station.

4. References

[1] Maxwell James Clerk, A Dynamical Theory of the Electromagnetic Field", Royal Society Transactions 155 (1865)

[2] Maxwell, James Clerk (1904), A Treatise on Electricity and Magnetism, Vol. II, Third Edition. Oxford University Press

[3] https://en.wikipedia.org/wiki/Finite-difference_time-domain_method

[4] https://en.wikipedia.org/wiki/Transmission-line_matrix_method

[5] T. Weiland, A Discretization Method for the Solution of Maxwell's Equations for Six-Component Fields, Electronics and Communications AEUE, vol. 31, no. 3, pp. 116–120, 1977

[6] K. Yee, « Numerical solution of initial boundary value problems involving Maxwell's equations in isotropic media », IEEE Transactions on Antennas and Propagation, vol. AP-16, pp. 302-307, 1966

[7] L. Gilles,.S. C. Hagness,. and L. Vazquez Comparison between Staggered and Unstaggered Finite-Difference Time-Domain Grids for Few-Cycle Temporal Optical Soliton Propagation Journal of Computational Physics 161, 379–400 (2000)

[8] R. Courant, K. Freidrichs and H. Lewy, « Uberdie partillenen differenzengleichungen der mathematischen physik », Mathematische Annalen, 100, 1928.

[9] T. Deveze, « Contribution à l'analyse, par différences finies, des équations de Maxwell dans le domaine temps », Thèse (Paris 6), 1992.

[10] IEC IEEE 62704 IEC/IEEE 62704-1 ED1: Determining the peak spatial-average specific absorption rate (SAR) in the human body from wireless communications devices, 30 MH to 6 GHz - Part 1: General requirements for using the finite difference time-domain (FDTD) method for SAR calculations

[11] Xu, X.G., Eckerman, K.F., 2010. "Handbook of Anatomical Models for Radiation Dosimetry Series in Medical Physics and Biomedical Engineering CRC.

[12] Fisher, H. L., Snyder, W. S., (1966), Annual progress report for period ending July 31 1966, Health Physics Division. Oak Ridge National Laboratory, Oak Ridge TN, USA, 1966.

[13] Hwang, J. M. L., Shoup R. L., Poston J. W., (1976), "Mathematical description of a one- and five-year-old child for use in dosimetry calculations," Oak Ridge National Laboratory, Oak Ridge TN, USA, 1976.

[14] Barber, P. W., Gandhi, O. P., Hagmann, M. J., Chatterjee, I., "Electromagnetic absorption in a multilayered model of man," IEEE Transaction on Biomedical Engineering, Vol. 26, No. 7, pp. 400-405, 1979.

[15] Cristy, “Mathematical phantoms representing children of various ages for use in estimates of internal dose,” Oak Ridge National Laboratory, Oak Ridge TN, USA, 1980.

[16] Lee et al., 2010

[17] Gandhi OP. Electromagnetic absorption in an inhomogeneous model of man for realistic exposure conditions. Bioelectromagnetics. 1982;3(1):81-90.

[18] Zankl, M., Veit, R., Williams, G., Schneider, K., Fendel, H., Petoussi, N., Drexler, G., (1988), “The construction of computer tomographic phantoms and their application in radiology and radiation protection,” Radiation and Environmental Biophysics, Vol. 27, pp. 153–164, 1988

[19] Petoussi-Henss, N., Zankl, M., (1998), “Voxel anthropomorphic models as a tool for internal dosimetry,” Radiation Protection Dosimetry, Vol. 79, pp. 415–418, 1998.

[20] http://www.nlm.nih.gov/research/visible/visible_human.html

[21] http://vkh3.kisti.re.kr/

[22] Shao-Xiang Zhang, Pheng-Ann Heng, Zheng-Jin Liu Chinese Visible Human Project: Dataset Acquisition and Its Primary Applications Proceedings of the 2005 IEEE Engineering in Medicine and Biology 27th Annual Conference Shanghai, China, September 1-4, 2005

[23] Park, J. S., Chung, M. S., Hwang, S. B., Lee, Y. S., Har, D. H., and Park, H. S., (2005), “Visible Korean Human: Improved Serially Sectioned Images of the Entire Body,” IEEE Transaction on Medical Imaging, Vol. 24, No. 3, pp. 352-360, 2005

[24] Xu, X. G., Chao, T. C., Bozkurt, A., (2000), “VIP-MAN: an image based whole-body adult male model constructed from color photographs of the Visible Human Project for multi-particle Monte Carlo calculations,” Health Physics, Vol. 78, pp. 476–485, 2000.

[25] http://visiblehuman.epfl.ch

[26] I. G. Zubal et al 1994 Computerized 3-dimentional segmented human anatomy. Med. Phy. 21, 299e302.

[27] M.J. Ackerman, (1995) Visible Human Project D-Lib. Mag. (www.nlm.nih.gov/research/visible/visible_human.html)

[28] Dimbylow, P. J., (1997), “FDTD calculations of the whole-body averaged SAR in an anatomically realistic voxel model of the human body from 1 MHz to 1 GHz,” Physics in Medicine and Biology, Vol. 42, pp. 479–490.

[29] P.J. Dimbylow, (2005) Development of the female voxel phantom, NAOMI and its application to calculations of induced current densities and electric fields from applied low frequency magnetic and electric fields. Phys. Med. Biol., 50(6):1047–1070, 2005

[30] Nagaoka, T., Watanabe, S., Sakurai, K., Kuneida, E., Watanabe, S., Taki, M., Yamanka, Y., (2004), “Development of realistic high resolution whole-body voxel models of Japanese adult male and female of average height and weight, and application of models to radio-

frequency electromagnetic-field dosimetry," Physics in Medicine and Biology, Vol. 49, pp. 1–15, 2004.

[31] Lee A K, Choi W Y, Chung M S, Choi H D and Choi J I 2006 Development of Korean male body model for computational dosimetry ETRI J. 28 107–10

[32] Kim C H, Choi S H, Jeong J H, Lee C and Chung M S 2008 HDRK-man: a whole body voxel model based on high resolution color slice images of a Korean adult male cadaver Phys. Med. Biol. 53 4093–106

[33] T. Wu et al., (2011). Chinese adult anatomical models and the application in evaluation of RF exposures. Phys. Med. Biol. 56, 2075

[34] A. Christ et al., 2010 The Virtual Family – development of surface-based anatomical models of two adults and two children for dosimetric simulations. Physics in Medicine and Biology, 55(2): N23–N38

[35] https://itis.swiss/virtual-population/virtual-population/overview/

[36] Lee A K & Choi H D 2023 Dosimetric assessment in the brain for downlink EMF exposure in Korean mobile communication networks Environmental Research 234, 116542

[37] N. Varsier et al., 2015 A novel method to assess human population exposure induced by a wireless cellular network. Bioelectromagnetics, 36(6), 451-463.